Corrosion Science 112 (2016) 338–346

Contents lists available at ScienceDirect

Corrosion Science

journal homepage: www.elsevier.com/locate/corsci

Oxidation behavior and microstructural decomposition of Ti-6Al-4V and Ti-6Al-4V-1B sheet

D.A. Brice[a,*], P. Samimi[a,e], I. Ghamarian[a,e], Y. Liu[b,e], R.M. Brice[b], R.F. Reidy[b], J.D. Cotton[c], M.J. Kaufman[d], P.C. Collins[a,e]

[a] Department of Materials Science and Engineering, Iowa State University, Ames, IA, 50011, United States
[b] Department of Materials Science and Engineering, University of North Texas, Denton, TX 76205, United States
[c] The Boeing Company, Seattle, WA, United States
[d] Department of Metallurgical and Materials Engineering, Colorado School of Mines, Golden, CO, 80401, United States
[e] The Center for Advanced Non-Ferrous Structural Alloys (CANFSA), A joint NSF I/UCRC between CSM and UNT, United States

ARTICLE INFO

Article history:
Received 6 February 2016
Received in revised form 26 July 2016
Accepted 30 July 2016
Available online 1 August 2016

Keywords:
A. Alloy
A. Titanium
B. TEM
B. SEM
C. Oxidation
Decomposition

ABSTRACT

A direct comparison between the oxidation behavior of Ti-6Al-4V and Ti-6Al-4V + 1B has been conducted to elucidate whether the addition of boron to Ti-6Al-4V impacts the oxidation behavior. Industrially prepared sheet of Ti-6Al-4V and Ti-6Al-4V + 1B were oxidized at temperatures between 650 and 950 °C for holding times of 25 and 50 h. Weight-gain measurements and characterization of surface and near-surface microstructures showed that the addition of 1 wt% B increased the material's oxidation resistance. Additionally, the ingress of oxygen tends to decrease the solubility of other alloying species in α-Ti and leads to the formation of a distinctive and atypical microstructure with a distinct morphology.

1. Introduction

Titanium and its alloys are known for being resistant to corrosion at relatively low temperatures due to the presence of a thin native oxide layer at the surface [1]. However, the performance of titanium alloys at high temperatures has always been limited owing to the gradual oxidation and subsequent degradation of the material. Applications of titanium alloys are often limited to temperatures below 550 °C, e.g., 400 °C for Ti-6Al-4V[1] [2], due to the growth of an oxide layer at temperatures above this mark and the concurrent transition of the oxide to a more active, non-protective state [3]. Ti-6Al-4V accounts for nearly 60% of titanium produced [4] and is used in a wide range of applications, from airframes to biomedical implants [2].

The oxidation of titanium and its alloys has been previously studied by several authors [5–9], including recent combinatorial studies of oxide formation and stability [10–13], and a general understanding of the oxidation process is present in the Refs. [10,13–15]. During high temperature exposure, oxygen, a strong α-stabilizing element, promotes the formation of a layer of oxygen-enriched α-phase near the surface, called the α-case. Following the formation of the α-case, the native oxide layer coarsens and evolves and can exhibit a non-uniform oxygen concentration throughout the oxide [16]. The consequences of the oxidation are: scale growth, the formation of cracks due to the evolution of compressive stress and ultimately material failure. Therefore, the formation of thick oxide scales is an important limiting factor for the service temperature of most commercially available titanium alloys.

Recently, attempts to improve the mechanical properties of Ti-6Al-4V have concluded that additions of boron (B) can improve certain mechanical properties, including creep and elastic strength [17–21]. Additionally, it is seen that the addition B affects the microstructure by promoting an α-phase morphology that is equiaxed, a morphology that is typically only obtained through thermomechanical working [22]. However, currently there is little understanding on boron's effect on the oxidation behavior of titanium, and must be investigated because boron may provide oxidation resistance to titanium alloys [23] and therefore increase their maximum service temperature. The addition of B to Ti alloys results in the formation TiB intermetallics particles, and the oxidation of TiB produces TiO_2 and B_2O_3. The production of B_2O_3 is problematic due to the fact that depending on temperature it

* Corresponding author.
E-mail address: dabrice@iastate.edu (D.A. Brice).

[1] All concentrations presented in this paper will be in weight%, consistent with low concentration Ti-based alloys

http://dx.doi.org/10.1016/j.corsci.2016.07.032

will form in liquid form and solidify into an amorphous phase or volatilize [24–27]. The evaporation of B_2O_3 has been linked to the cracking within the material, and has led some to believe that the formation of B_2O_3 does not account for the oxidation resistance afforded by B in Ti alloys [25]. Thus, to understand the influence that B may play on the oxidation behavior of Ti-6Al-4V, this paper presents a direct comparison of the oxidation behavior of industrially supplied Ti-6Al-4V and Ti-6Al–4 + 1B sheet for temperatures ranging from 650 °C–950 °C. The oxidation tests were carried out for different holding times in an attempt to understand whether the inclusion of boron in titanium alloys are beneficial to oxidation resistance.

2. Experimental procedure

Industrially supplied sheet materials of Ti-6Al-4V and Ti-6Al-4V-1B, received from Boeing, were used in this study. The composition of Ti-6Al-4V and Ti-6Al-4V-1B are presented in Table 1. Compositions were determined by Luvak Laboratories, Inc. (Boylston, MA) according to the following ASTM standards: ASTM E 1941-10 for carbon, ASTM E 1447-09 for hydrogen, ASTM E 1409-13 for oxygen and nitrogen, and ASTM 2371-13 for all remaining species.

Nine specimens with the dimension of 13 mm × 13 mm × 1 mm were cut from each sheet. Prior to heat-treatment, the specimens were prepared following conventional metallographic techniques using an auto polishing MultiPrep™ system (Allied High Tech, CA, USA) with SiC abrasive papers whose grit size ranged from 120 to 800. Following grinding, the specimens were cleaned ultrasonically, successively moving from acetone to distilled water to ethanol and finally, to methanol. The specimens were ultrasonicated for 5 min at each step. After cleaning, 8 of the specimens were placed in a vacuum furnace (at 50 °C) to dry for 20 min, and weighed using an OHAUS Discovery microbalance, with a precision of ±0.03 mg, while the 9th was retained in the as-received condition. The specimens were placed in alumina crucibles, and oxidized at 4 different temperatures (650 °C, 750 °C, 820 °C, and 950 °C) for 2 different times for each temperature (25 and 50 h). These temperatures represent temperature targets set by industry (i.e., 650 °C and 820 °C) as well as additional temperatures to better understand the oxidation behavior (750 °C and 950 °C). Following the oxidation exposures, all the specimens were air-cooled to room temperature. After air-cooling, the specimens were reweighed.

Following oxidation and reweighing, the oxidized specimens were cut in half to reveal the cross-section of the oxidized surface, and mounted in conductive C-based Phenol using a TechPress2™ (Allied High tech, USA). After mounting, the cross-sections of the specimens were ground using SiC abrasive papers whose grit size ranged from 600 to 800. The specimens were fine-polished with 0.04 μm colloidal silica suspension.

Scanning electron microscopy (SEM) studies were carried out using an FEI Nova 230 NanoSEM field emission gun scanning electron microscope equipped with an electron backscattered detector. Specimens for TEM were prepared using an FEI Nova Nanolab 200 DualBeam™ focused ion beam (FIB)/SEM. These site-specific TEM specimens were subsequently analyzed in an FEI Tecnai G2 F20 STEM field emission gun scanning transmission electron microscope operating at 200 keV. The TEM was equipped with an HAADF STEM (high angle annular dark field)detector and an energy dispersive x-ray spectrometer.

3. Results and discussion

The results from the weight change measurements, presented in Fig. 1, show a weight increase for all specimens. This weight gain is attributed to both oxygen incorporated into the surface oxide and dissolved oxygen in the Ti-6Al-4V and Ti-6Al-4V-1B sheet. From these weight measurements it is clear that: (1) the addition of boron into Ti-6Al-4V retards weight gain, consistent with observations reported by Luan et al. [23], (2) the difference in weight gain at a given temperature for the two exposure times is more pronounced in the Ti-6Al-4V specimens than those in which boron has been added, and (3) at an undetermined temperature at or above 820 °C, there is a marked increase in the weight gain rate for all specimens.

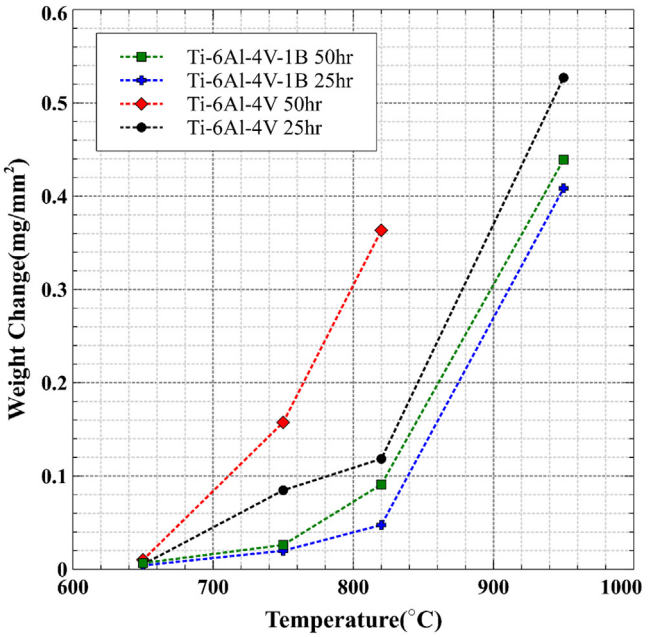

Fig. 1. Weight change of Ti-6Al-4V and Ti-6Al-4V + 1B sheet as a function of oxidation temperature for 25 and 50 h. The uncertainty associated with the weight change is±0.003 g.

As a reference, an SEM backscattered electron micrographs of the as-received microstructures of the Ti-6Al-4V and Ti-6Al-4V-1B are shown in Fig. 2(a,b) respectively. Oxidation-induced microstructural changes were assessed by collecting backscattered electron SEM micrographs for both alloys at temperatures ranging from 750 °C to 950 °C, and are presented in Figs. 3 (a–f) and 4 (a–f) for the two holding times, 25 and 50 h, respectively. Micrographs from specimens oxidized at 650 °C are not reported due to the fact that no clear microstructural change can be seen near the surface. For specimens oxidized at 750 °C and 820 °C, there is a clear decrease in the β-phase volume fraction below the oxide metal interface. This is indicative of the formation of the α-case due to oxygen ingress. The phase fractions from the Ti-6Al-4V and Ti-6Al-4V + 1B specimens have been analyzed using standard stereographic procedures developed and subsequently captured using MIPAR [28–30] and are presented in Fig. 5. It is clear from Fig. 5 that the formation of the oxygen-stabilized α-case consequently decreases the local β-phase fraction in areas adjacent to the oxidized surface.

Looking at the oxide scale adherent to the material one can see a pronounced difference in oxidation resistance between Ti-6Al-4V and Ti-6Al-4V-1B. From Fig. 6(a) one can see the oxide scale has separated from the Ti-6Al-4V substrate (see Fig. 6(a)), in contrast the Ti-6Al-4V-1B (see Fig. 6(b)) has a well adhered oxide scale and the metallic substrate has not been depleted to the extent that Ti-6Al-4V has been. When considering these results along with the weight measurements (see Fig. 1) it is clear that the addition of B to Ti-6Al-4V alloy has improved the oxidation resistance of the alloy.

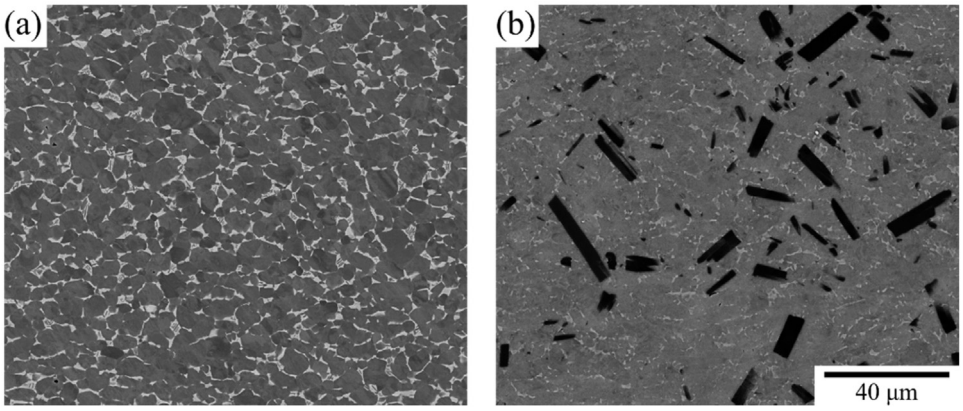

Fig. 2. SEM backscattered images of the as received sheet material (a) Ti-6Al-4V and (b) Ti-6Al-4V + 1B.

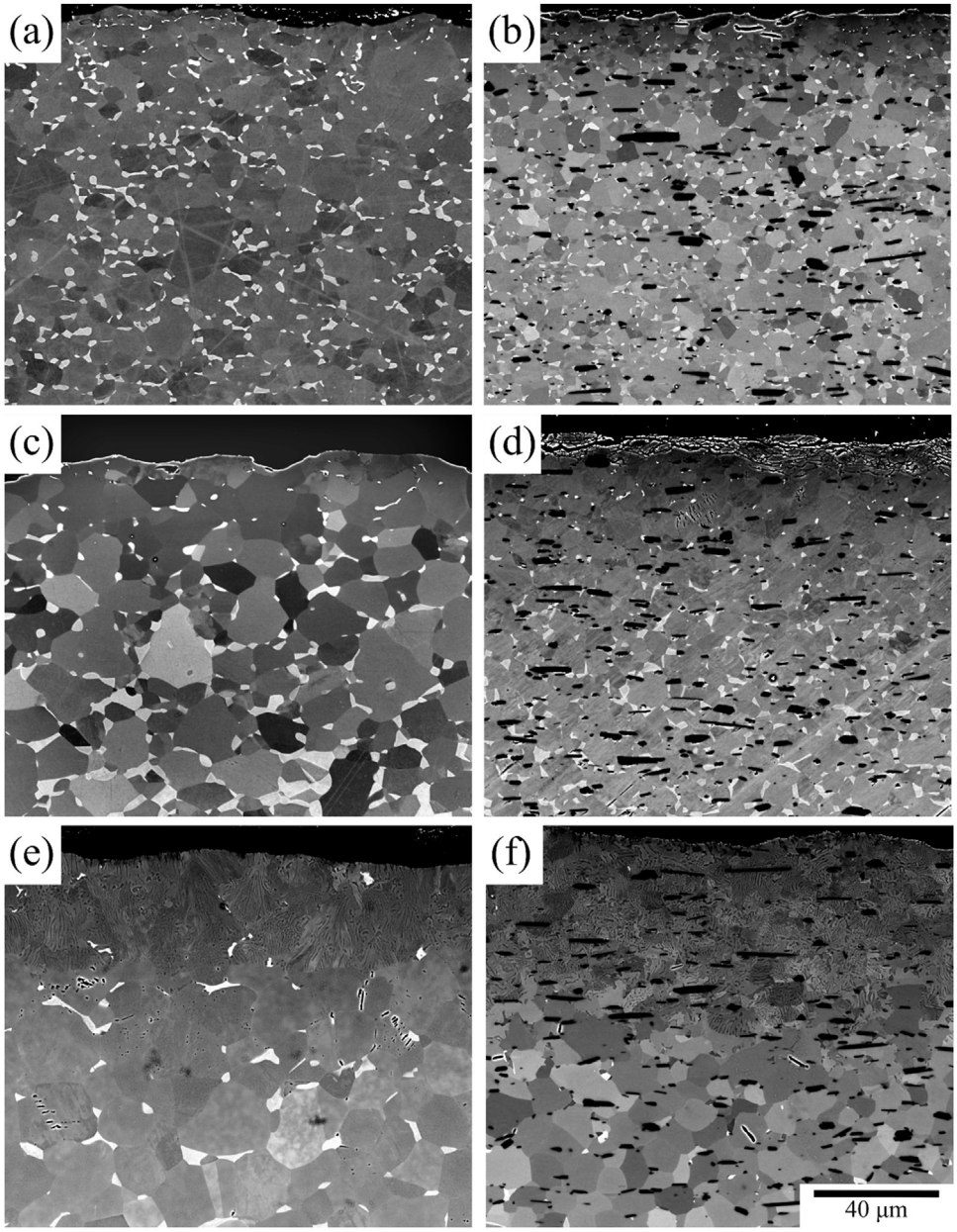

Fig. 3. SEM backscattered electron micrographs showing the microstructural change caused by oxygen ingress into the specimens of Ti64 (a) 750 °C (c) 820 °C (e) 950 °C for 25 h and Ti64 + 1B(b) 750 °C (d) 820 °C (f) 950 °C for 25 h.

Table 1
Measured composition of industrially supplied sheet of Ti-6Al-4V and Ti-6Al-4V + 1B. All concentrations in mass percent.

	Al ± 0.12%	V ± 0.08	Fe ± 0.005	C ± 0.005	H ± 0.0005	N ± 0.002	O ± 0.005	B ± 0.05	Ti
Ti-6Al-4V	6.17	4.08	0.16	0.025	0.0052	0.016	0.188	0	balance
Ti-6Al-4V + 1B	6.61	4.1	0.06	0.43	–	0.17	0.13	0.97	balance

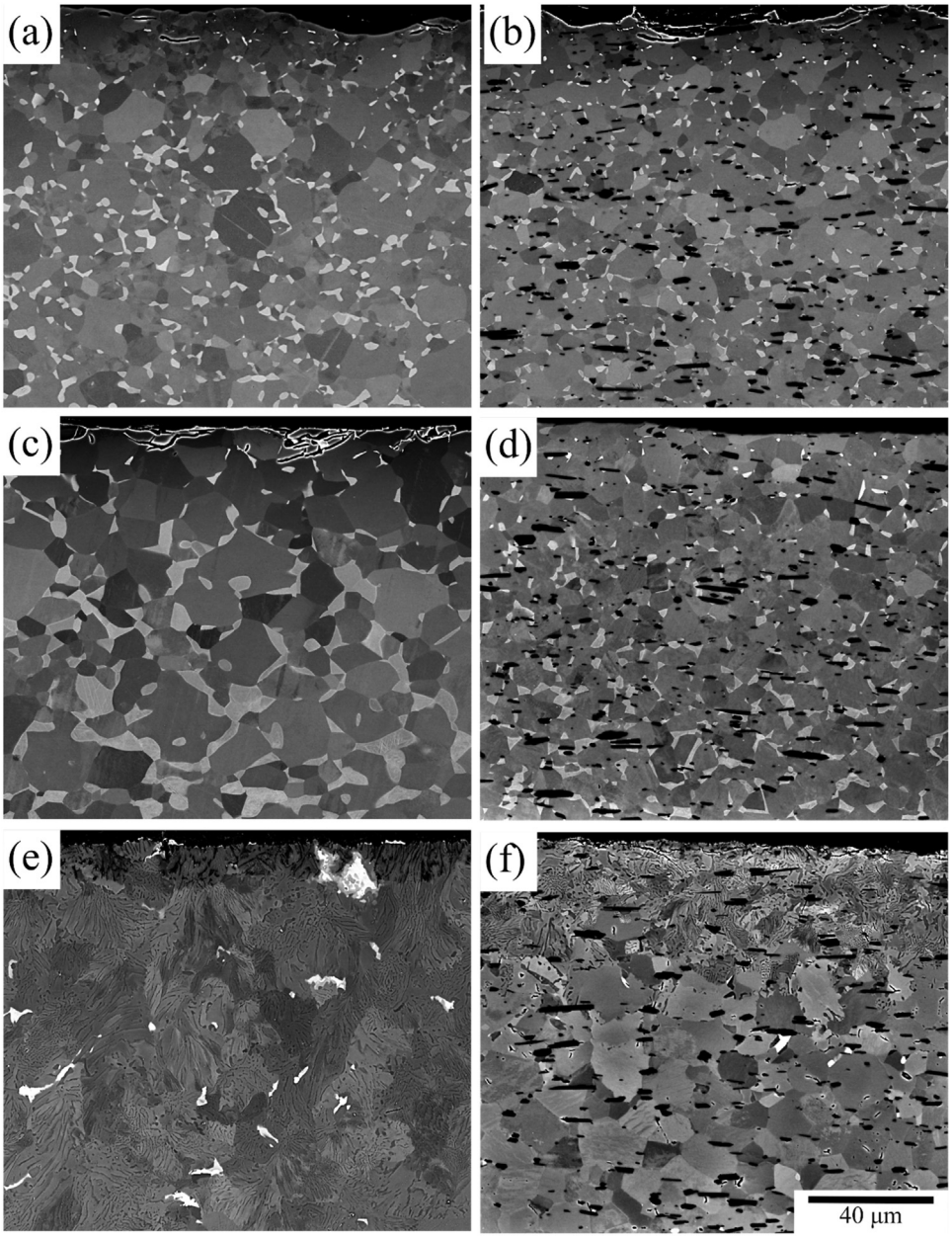

Fig. 4. SEM backscattered electron micrographs showing the microstructural change caused by oxygen ingress into the specimens of Ti64 (a) 750 °C (c) 820 °C (e) 950 °C for 50 and Ti64 + 1B(b) 750 °C (d) 820 °C (f) 950 °C for 50 h.

In addition, the specimens exposed to 950 °C indicate that a new microstructural feature has formed just below the metal/oxide interface (see Figs. 3 (e,f) and 4 (e,f)). This feature, which is presented more clearly at higher magnification images shown in Fig. 7(a,b), is characterized by a prototypical length scale and aspect ratio (often oriented away from the surface) yet does not exhibit any other regular geometric order that would be associated with crystallographically distinct precipitates such as faceted (i.e., coherent) interfaces. This seemingly co-continuous feature is indicative of a decomposition-like structure, likely caused by the chemical change arising from the ingress of oxygen. The depth to which this decomposition structure extend into the material from the oxide metal interface is greater for Ti-6Al-4V compositions than those with boron additions. The formation and development of this microstructure just below the surface indicates that it is a direct consequence of oxygen ingress into the base metal during oxidation.

Because the decomposition structure is characterized by spatial variations in brightness in the backscattered SEM images (see Fig. 7(a,b)), which is likely associated with differences in the aver-

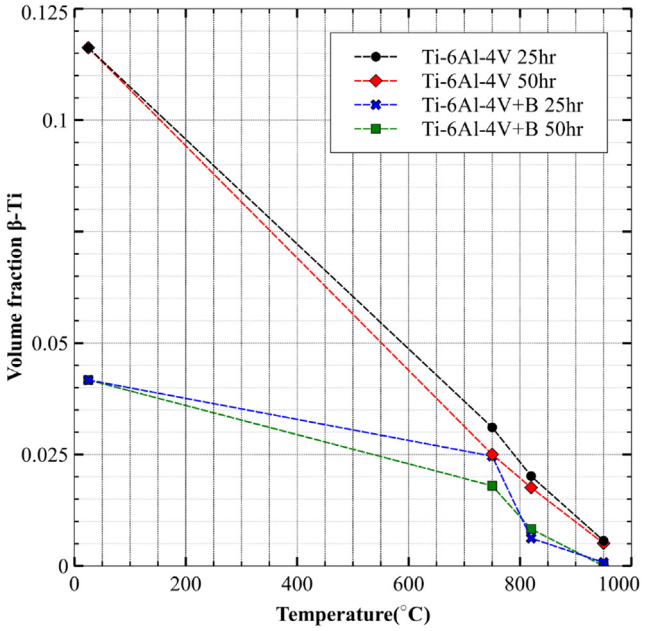

Fig. 5. Variation of β-phase fraction as a function of temperature for Ti-6Al-4V andTi-6Al-4V + B oxidized at 25 and 50 h of regions adjacent to the metal oxide interface and penetrating 20 μm into the material.

age atomic mass, energy dispersive spectroscopy (EDS) was used in SEM to collect composition maps (see Fig. 8(b–f)) in order to determine the relative partitioning behavior of the constituent elements. From such composition maps, it is clear that the Al and V are segregating into the dark features, and the bright features which are most likely the parent matrix is composed of primarily Ti and O. It should be noted that the solubility of B in both *hcp* α and *bcc* β titanium is very small and below the detection limit of EDS. Thus, no measurable amount of B is detected in either the bright or dark features of the decomposition structure, but rather seems to reside exclusively within the TiB particles.

These results have been considered and are presented in context with the expected changes in elemental partitioning due to oxygen, which have been calculated using PANDAT™ [31] (see Fig. 9). From Fig. 9, it is seen that the addition of oxygen into a binary titanium mixture results in the expulsion of the various common alloying element species (including Al and V) out of the α-phase. This oxygen-induced rejection of elements has been linked to other unusual phase transformations [10]. Thus, these observations indicate that the change in the Al and V solubility of α-phase in Ti-6Al-4V triggers the formation of this decomposition microstructure.

In order to analyze the structure and composition of the newly formed decomposition microstructure in the subsurface region of the specimens oxidized at 950 °C for 25 h, a TEM foil was prepared and analyzed. The STEM image (Fig. 10(a)) and the corresponding STEM-EDS maps of the alloying elements confirms that the decomposition microstructure is composed of two chemically distinct phases. It is evident that phase with darker contrast in the STEM image has a larger concentration of Al and V compared with the bright phase (the matrix), which is enriched in Ti and O. This further supports the hypothesis that the decomposition structure has formed due to oxygen ingress into the material, and shows that oxygen expels other species (here, both a beta stabilizer (V) and an alpha stabilizer (Al)) from the oxygen-stabilized (and parent) α-

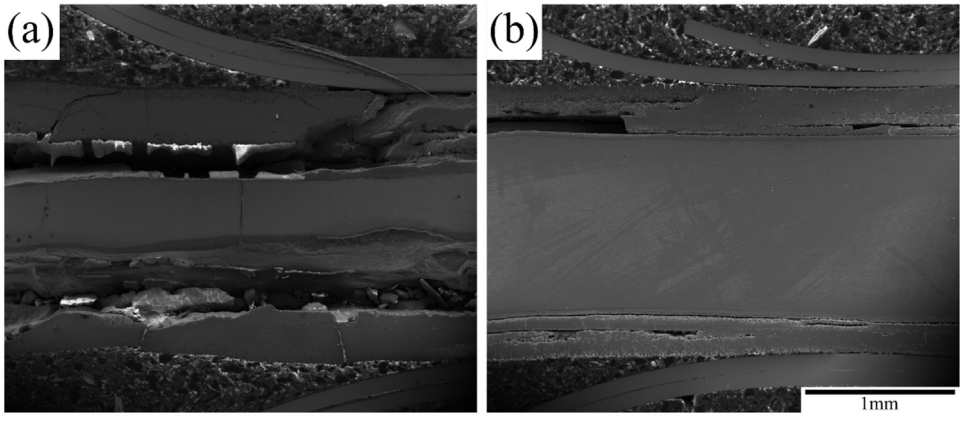

Fig. 6. Oxide scale formed after 950 °C 50hr on (a) Ti-6Al-4V and (b) Ti-6Al-4V-1B.

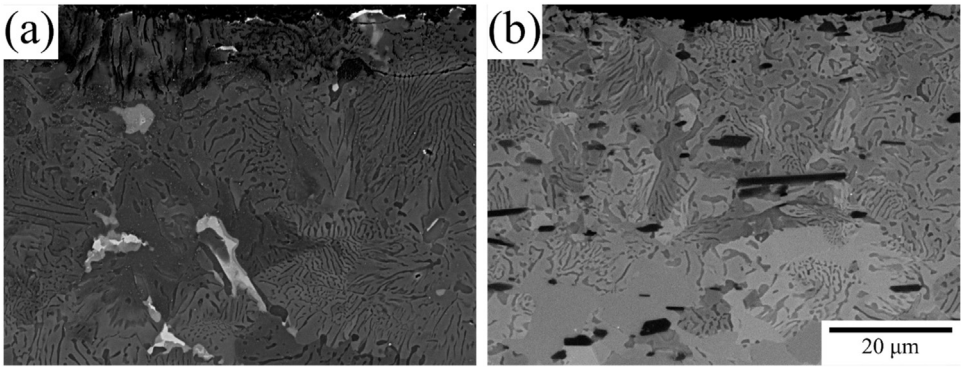

Fig. 7. High magnification SEM backscatter images from the decomposed structure adjacent to the metal oxide interface from (a) Ti-6Al-4V and (b) Ti-6Al-4V-1B.

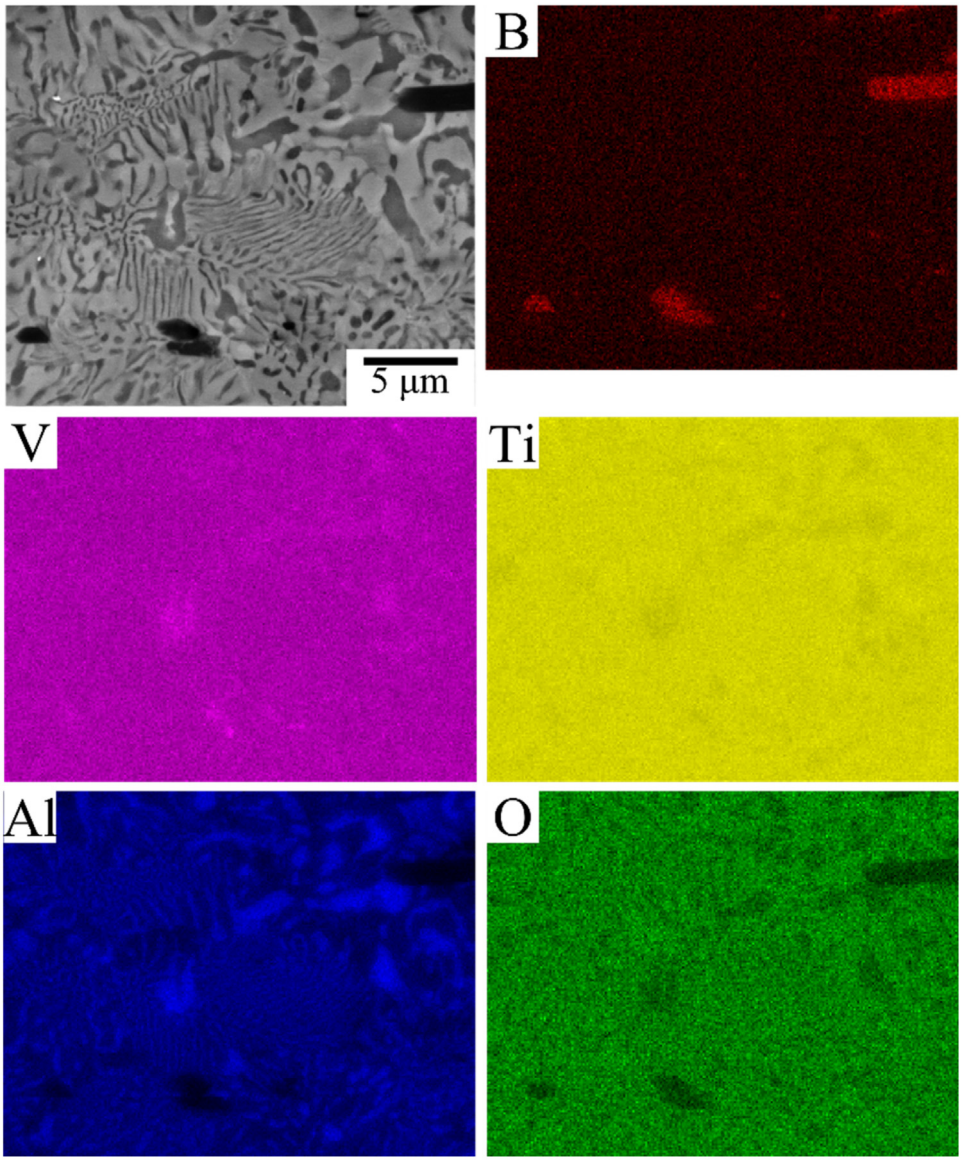

Fig. 8. Elemental maps of B, V, Ti, Al and O for Ti-6Al-4V-1B heat-treated at 950 °C for 25 h.

phase. The result of compositional assessment is in accordance with PADANT^{TM} calculations shown in Fig. 9. Interestingly, the quantification of the STEM-EDS results indicate that the composition of the darker phase is ~22 at.% Al, ~3 at.% V which is consistent with the composition of Ti_3Al as reported in the literature [32–34]. In order to confirm the darker phase in the decomposition structure (see Fig. 5(a)) corresponds to Ti_3Al, a selected area diffraction pattern was obtained from this phase, shown as an inset in Fig. 10(a) which can be consistently indexed as $\left[01\bar{1}1\right]$ zone axis of Ti_3Al intermetallic compound with the hcp structure of DO_{19} type. The PANDAT^{TM} calculations presented in Fig. 11 show that the addition of O into an alloy composition similar to those presented in this study can cause the formation of Ti_3Al. Given that literature has reported that Ti_3Al is a highly non-stoichiometric intermetallic phase which has a large solubility for V, it is not unreasonable to expect the formation of Ti_3Al rich in V as consequence of oxidation as presented previously above. The mechanism for the microstructural evolution is not clear, but the features are consistent with discontinuous precipitation [35–37], which has been reported previously for oxidation of Ti-Mo alloys [10]. In discontinuous precipitation, it is possible for the parent phase to give rise to a new compositionally different, crystallographically identical child phase, as well as precipitate a new phase. It is suggested here that one possible mechanism for the evolution of this microstructure is the discontinuous precipitation sequence, given below:

$$\alpha^{O-lean} + O_{dissolved} \rightarrow \alpha^{O-rich} + \alpha_2^{Al,V-rich} \quad (1)$$

Thus far, it has been shown that a new microstructure with distinct morphology has formed as a consequence of oxygen ingress and the resulting phases are oxygen enriched α-Ti and Ti_3Al. In addition, it has been shown that B does play a role on the rate of oxygen ingress and the concurrent depth to which this new microstructural feature is formed. Unfortunately, the role of B in the oxidation process is still not understood, nor have the results here shed any mechanistic insights. It is known that boron has a low solubility in both α-Ti and β-Ti and has been measured to be a fast diffuser in α-Ti [38]. These two features would suggest that B should not be a rate limiting factor to oxidation; however, the notable influence on lowering weight gain, the reduction in scale growth and microstructural changes indicate that B plays a dominant role. There are two possibilities that are presented here as hypotheses. Firstly, the fact that B changes the nature of the oxide

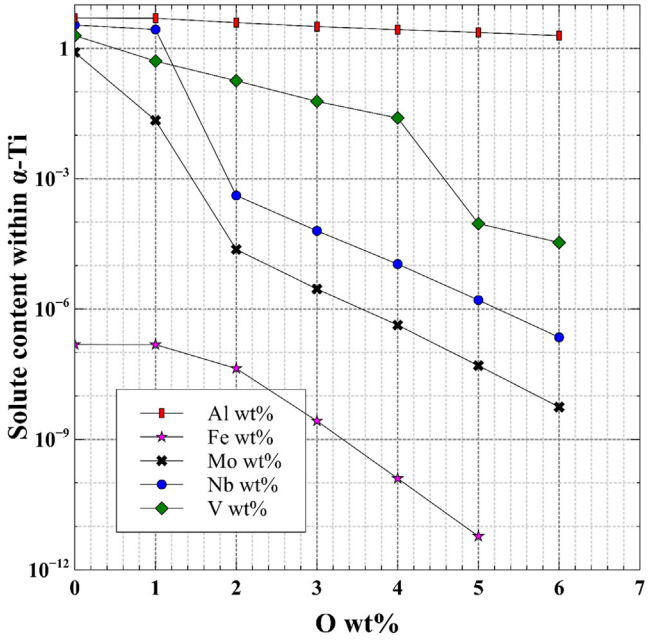

Fig. 9. Calculated concentrations of various species in α-Ti in relation to oxygen content using PANDAT™.

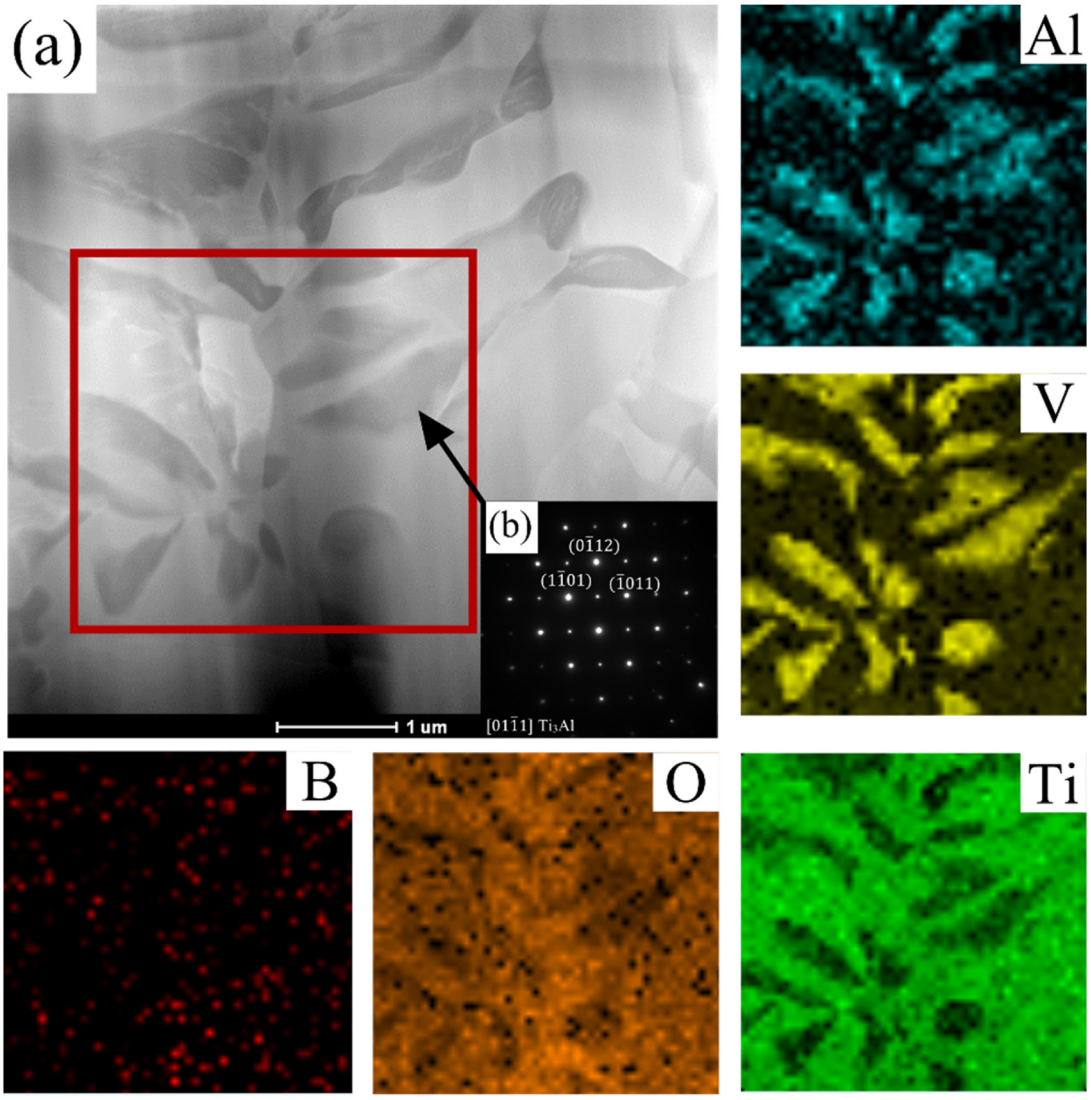

Fig. 10. Analysis of the decomposition structure below the metal/oxide interface on the Ti-6Al-4V-1B specimen heat-treated to 950 °C for 50 h. (a) STEM image of the area surveyed, the area within the square represents the area analyzed with STEM-EDS. (b) Selected area diffraction of the dark features within the decomposition structure.

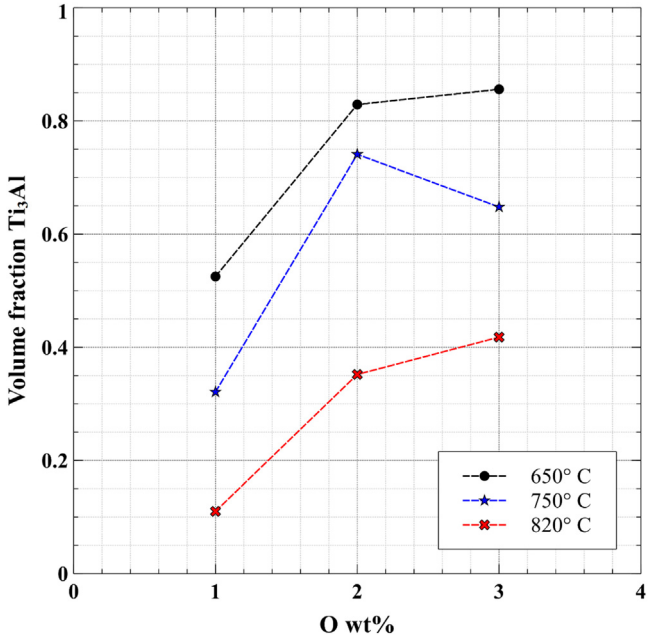

Fig. 11. PANDAT calculated volume fraction of Ti_3Al in relation to oxygen increasing content in a Ti-6Al-4V + 1 B composition at 650 °C, 750 °C, and 820 °C.

scale (thinner, more adherent, fewer cracks) may 'turn off' oxygen sources (i.e., the oxide cracks), reducing the oxygen ingress and subsequent decomposition. Secondly, B may behave in a manner that influences the vacancy concentration, thus restricting O transport in either the oxide layer or in the base material.

4. Conclusions

A comparison between of the oxidation behavior of Ti-6Al-4V with and without addition of B was conducted at different temperatures. It is shown that the addition of 1 wt% B into Ti-6Al-4V causes a marked increase in oxidation resistance of the material according to weight gain measurements of the specimens and evolution of the microstructural in the subsurface region. The ingress of oxygen causes the decomposition of the α-phase into an oxygen enriched α-Ti and α_2-Ti_3Al at the oxidation temperature of 950 °C. It is concluded from compositional measurement and thermodynamic calculations that the phase decomposition is caused by solubility decrease of alloying species in α-Ti as a consequence of oxygen ingress. The role of B in improving of the oxidation resistance is still not well understood.

Acknowledgments

This work was conducted as part of an REU supplement to the NSF I/UCRC Center for Advanced Non-Ferrous Structural Alloys (CANFSA) which is a joint industry-university center between the Colorado School of Mines and the Iowa State University. The authors gratefully acknowledge the support of NSF (award number 1641143) and the support and active mentorship of the industrial partners. The authors also gratefully acknowledge the facilities available at the University of North Texas' Center for Advanced Research and Technology (CART).

References

[1] J. Pan, D. Thierry, C. Leygraf, Electrochemical impedance spectroscopy study of the passive oxide film on titanium for implant application, Electrochim. Acta 41 (1996) 1143–1153.
[2] R.W. Boyer, E.W. Gerhard Collings, Materirals Properties Handbook Titanium Alloys, ASM International, 1994.
[3] G.W.J.C. Lutjering, Titanium, Springer-Verlag, Berlin, 2007.
[4] R.R. Boyer, An overview on the use of titanium in the aeros, Mater. Sci. Eng.: A A213 (1996) 103–114.
[5] A.J.B.B.P.F. Stratton, Case hardening titanium, in: I International Surface Engineering Congress and the 13th IFHTSE Congress, ASM International Columbus, Ohio, 2002, pp. 22–28.
[6] S. Zabler, Interstitial Oxygen diffusion hardening — a practical route for the surface protection of titanium, Mater. Charact. 62 (2011) 1205–1213.
[7] R.K. Wallace, The effect of oxidation on the mechanical properties of Beta-21s, in: R. Eylon (Ed.), Beta Titanium Alloys in the 1990's, Minerals, Metals & Materials Society, 1993.
[8] T.A. Wallace, R.K. Clark, K.E. Wiedemann, Oxidatoin characteristics of beta21 s in air in the temperature range 600–800 °C, in, National Aeronautics and Space Administration (NASA), Hampton, VA (United States), Langley Res. Center (1992).
[9] J.L. Murray, H.A. Wriedt, The O-Ti (oxygen-titanium) system, Bull. Alloy Phase Diagr. 8 (1987).
[10] P. Samimi, Y. Liu, I. Ghamarian, P.C. Collins, A novel tool to assess the influence of alloy composition on the oxidation behavior and concurrent oxygen-induced phase transformations for binary Ti–xMo alloys at 650 °C, Corros. Sci. 89 (2014) 295–306.
[11] P. Samimi, Y. Liu, I. Ghamarian, D.A. Brice, P.C. Collins, A new combinatorial approach to assess the influence of alloy composition on the oxidation behavior and concurrent oxygen-induced phase transformations for binary Ti–xCr alloys at 650 °C, Corros. Sci. 97 (2015) 150–160.
[12] P. Samimi, D.A. Brice, R. Banerjee, M.J. Kaufman, P.C. Collins, On the influence of alloy composition on oxidation performance and oxygen-induced phase transformations in Ti-(0–8)wt%Al alloys, Rev. Resubmitted J. Mater. Sci. (Dec 2015).
[13] Y. Liu, P. Samimi, I. Ghamarian, D. Brice, D. Huber, Z. Wang, V. Dixit, S. Koduri, H. Fraser, P. Collins, Discovery via integration of experimentation and modeling: three examples for titanium alloys, JOM 67 (2015) 164–178.
[14] J.W. Fergus, Review of the effect of alloy composition on the growth rates of scales formed during oxidation of gamma titanium aluminide alloys, Mater. Sci. Eng.: A 338 (2002) 108–125.
[15] E. McCafferty, J.P. Wightman, An X-ray photoelectron spectroscopy sputter profile study of the native air-formed oxide film on titanium.pdf, Appl. Surf. Sci. 143 (1999) 92–100.
[16] R. Padma, K. Ramkumar, M. Satyam, Growth of titanium oxide overlayers by thermal oxidation of titanium, J. Mater. Sci. 23 (1988) 1591–1597.
[17] O.O. Bilous, L.V. Artyukh, A.A. Bondar, T.Y. Velikanova, M.P. Burka, M.P. Brodnikovskyi, O.S. Fomichov, N.I. Tsyganenko, S.O. Firstov, Effect of boron on the structure and mechanical properties of Ti–6Al and Ti–6Al–4 V, Mater. Sci. Eng.: A 402 (2005) 76–83.
[18] S. Roy, S. Suwas, S. Tamirisakandala, D.B. Miracle, R. Srinivasan, Development of solidification microstructure in boron-modified alloy Ti–6Al–4V–0.1B, Acta Mater. 59 (2011) 5494–5510.
[19] G. Singh, D.V.V. Satyanarayana, R. Pederson, R. Datta, U. Ramamurty, Enhancement in creep resistance of Ti–6Al–4 V alloy due to boron addition, Mater. Sci. Eng.: A 597 (2014) 194–203.
[20] S. Tamirisakandala, R.B. Bhat, J.S. Tiley, D.B. Miracle, Grain refinement of cast titanium alloys via trace boron addition, Scr. Mater. 53 (2005) 1421–1426.
[21] J. Zhu, A. Kamiya, T. Yamada, W. Shi, K. Naganuma, Influence of boron addition on microstructure and mechanical properties of dental cast titanium alloys, Mater. Sci. Eng.: A 339 (2003) 53–62.
[22] D. Hill, R. Banerjee, D. Huber, J. Tiley, H.L. Fraser, Formation of equiaxed alpha in TiB reinforced Ti alloy composites, Scr. Mater. 52 (2005) 387–392.
[23] J. Luan, Z. Jiao, G. Chen, C. Liu, Improved ductility and oxidation resistance of cast Ti–6Al–4 V alloys by microalloying, J. Alloys Compd. 602 (2014) 235–240.
[24] Y.H. Koh, S.Y. Lee, H.E. Kim, Oxidation behavior of titanium boride at elevated temperatures, J. Am. Ceram. Soc. 84 (2001) 239–241.
[25] E. Zhang, G. Zeng, S. Zeng, Oxidation behavior of in situ TiB short fibre reinforced Ti-6Al-1.2B alloy in air, J. Mater. Sci. 37 (2002) 4063–4071.
[26] T.S.R.C. Murthy, R. Balasubramaniam, B. Basu, A.K. Suri, M.N. Mungole, Oxidation of monolithic TiB2 and TiB2-20 wt.% MoSi2 composite at 850 °C, J. Eur. Ceram. Soc. 26 (2006) 187–192.
[27] D. Lee, Y. Lee, D.J. Kim, The oxidation of TiB2 ceramics containing Cr and Fe, Oxid. Met. 56 (2001) 177–189.
[28] J.M. Sosa, Development of tools for 2D and 3D microstructural characterization and their application to titanium alloy microstructures, in: Materials Science and Engineering, The Ohio State University, Columbus, OH, 2015.
[29] J.M. Sosa, D.E. Huber, B. Welk, H.L. Fraser, Development and application of MIPAR™: a novel software package for two- and three-dimensional microstructural characterization, Integr. Mater. Manuf. Innov. 3 (2014) s1.
[30] P.C. Collins, B. Welk, T. Searles, J. Tiley, J.C. Russ, H.L. Fraser, Development of methods for the quantification of microstructural features in α+β-processed α/β titanium alloys, Mater. Sci. Eng.: A 508 (2009) 174–182.
[31] L.L.C. CompuTherm, Pandat 8.0-Phase Diagram Calculation Software for Multi-component Systems, CompuTherm LLC, Madison, WI, 2008, pp. 53719.
[32] K. Das, P. Choudhury, S. Das, The Al-O-Ti (aluminum-oxygen-titanium) System, J. Phase Equilibria 23 (2002).
[33] V. Raghavan, Al-Ti-V (aluminum-titanium-vanadium), J. Phase Equilibria Diffus. 26 (2005) 276–279.

[34] J.C. Schuster, M. Palm, Reassessment of the binary aluminum-titanium phase diagram, J. Phase Equilibria Diffus. 27 (2006) 255–277.
[35] J.-C. ZHAO, M.R. NOTIS, Spinodal decomposition ordering transformation, and discontinuous precipitation an a Cu-15Ni-8Sn alloy, Acta Mater. 46 (1998) 4203–4218.
[36] D.B. Williams, E.P. Butler, Grain boundary discontinuous precipitation reactions, Int. Metals Rev. 26 (1981) 153–183.
[37] H. Mats, On theories of growth during discontinuous precipitation, Metall. Trans. 3 (1972) 2729–2741.
[38] S. Divinski, F. Hisker, T. Wilger, M. Friesel, C. Herzig, Tracer diffusion of boron in α-Ti and γ-TiAl, Intermetallics 16 (2008) 148–155.